Spontaneous polarization as a Berry phase of the Hartree-Fock wave function: The case of $KNbO_3$

Sergio Dall'Olio and Roberto Dovesi
Gruppo di Chimica Teorica, Università di Torino, via Pietro Giuria 7, I-10125 Torino, Italy

Raffaele Resta
INFM, Dipartimento di Fisica Teorica, Università di Trieste, Strada Costiera 11, I-34014 Trieste, Italy
(Received 2 May 1997)

We have investigated the ferroelectric polarization of the perovskite oxide $KNbO_3$ within the self-consistent Hartree-Fock (HF) method, where the crystalline orbitals are expanded over a set of localized functions. According to the modern theory, macroscopic polarization is a geometric quantum phase: here we show that—within the HF framework—polarization can be cast as a Berry phase of Slater determinants. We calculate this observable for $KNbO_3$ in its tetragonal phase. Besides polarization, we investigate several other properties of the electronic ground state, including the broken-symmetry instability of the tetragonal structure. We therefore assess the reliability and the predictive power of the HF approach when dealing with this material, which is a paradigmatic case of intermediate ionic/covalent crystal. [S0163-1829(97)03739-9]

I. INTRODUCTION

We implement here the Berry phase theory of macroscopic polarization[1,2] within the *ab initio* Hartree-Fock (HF) scheme for crystalline solids, using the same general framework and the same computational techniques as in Ref. 3. Previous implementations were mostly performed at the level of density-functional theory[4] (DFT); there is only one published study of macroscopic polarization at the HF level, dealing with a rather simple crystal, in a computational setting quite different from the present one.[5] Other existing implementations concern oversimplified tight-binding models. The theory itself is available in a comprehensive review paper,[2] whose presentation emphasizes the DFT viewpoint. Though several features of the theory can be easily translated from DFT to HF by means of a pure change of semantics, there is an important conceptual difference: the HF scheme provides an explicit (single-determinant) many-body wave function for the crystalline electrons. This fact allows us to present the Berry phase theory of polarization in a more compact and elegant form than in the DFT-oriented literature, as we are going to show in Sec. II of this paper.

We have chosen to investigate the spontaneous polarization of the ferroelectric perovskite $KNbO_3$: this was in fact the very first material where spontaneous polarization could be theoretically accessed from a quantum-mechanical viewpoint.[6] Since that pioneering work, several papers—all of them within DFT—have thoroughly investigated features related to macroscopic polarization[7–10] and other structural and electronic properties of this material.[11–15] A recent paper studies the ferroelectric instability within a semiempirical HF method.[16] It is also worth mentioning that $KNbO_3$ has one of the highest values of the spontaneous polarization measured in nature.[17] Because of the above reasons, the perovskite $KNbO_3$ constitutes an ideal benchmark for our present HF implementation of the modern theory of polarization.

Besides providing a study of macroscopic polarization, we also provide here a comprehensive study of the structural and electronic properties of $KNbO_3$ within the HF scheme, including an investigation of the ferroelectric structural instability. Our results will be compared with those previously obtained by several authors within DFT.

The present implementation[18] makes use of the CRYSTAL95 code[19] and has been grafted on it. The HF crystalline orbitals are expanded as a linear combination of Bloch functions, and are evaluated over a regular three-dimensional mesh in reciprocal space. We show in Sec. III how to cope with these two aspects of the numerical implementation.

In Sec. IV we present several results giving insight into the electronic ground state of $KNbO_3$ at the HF level, both for the experimental ferroelectric geometry (in the tetragonal phase) and for a parent centrosymmetric geometry. In Sec. V we discuss the spontaneous symmetry breaking and the ferroelectric instabilty, whose theoretical description requires some care in the choice of technical ingredients. In Sec. VI we discuss our Berry phase calculations and we compare the resulting macroscopic polarization with the available experimental and theoretical data. Tests of numerical stability are also provided. In Sec. VII we draw our main conclusions.

II. BERRY PHASE OF SLATER DETERMINANTS

Quite generally, we are interested in the difference $\Delta\mathbf{P}$ in macroscopic polarization between two different structures of a crystalline solid. Typically one of the structures is centrosymmetric, such that $\Delta\mathbf{P}$ can be interpreted as the ''spontaneous polarization'' of the low-symmetry structure. In the Born-Oppenheimer approximation we can separate the electronic and ionic terms, and we focus on the former one $\Delta\mathbf{P}_{\rm el}$ in the following; the classical ionic term is almost trivial.[2] We assume that one can continuously transform the crystal from one structure to the other by switching a parameter λ (which controls the ionic coordinates) in the electronic Hamiltonian. Since a polarization difference is equivalent to the time integral of an electric current, our viewpoint closely

parallels the way spontaneous polarization is experimentally accessed: a typical measurement is in fact performed via polarization reversal, and its raw output is precisely the amount of current flowing through the sample while the ions flip from one structure to another.[20]

Without loss of generality we take λ to be dimensionless, and assuming the values of 0 and 1 for the two structures:

$$\Delta\mathbf{P}_{\rm el}=\mathbf{P}_{\rm el}(1)-\mathbf{P}_{\rm el}(0)=\int_0^1 d\lambda\ \mathbf{P}'_{\rm el}(\lambda). \tag{1}$$

Furthermore we assume that the crystal remains an insulator for all values of λ (i.e., the HF gap does not close), and that the macroscopic field vanishes along the transformation. This latter fact ensures that the Fock operator of the system is lattice periodic at any λ, and that the HF crystalline orbitals have the Bloch form:

$$\psi_s^{(\lambda)}(\mathbf{r},\mathbf{k})=e^{i\mathbf{k}\cdot\mathbf{r}}u_s^{(\lambda)}(\mathbf{r},\mathbf{k}), \tag{2}$$

where the u's are cell-periodic functions of $\mathbf{r}$. We assume the ψ's and the u's normalized to one over the crystal cell. It is furthermore convenient to choose the phases in such a way that $\psi_s^{(\lambda)}(\mathbf{r},\mathbf{k})$ is a periodic function of $\mathbf{k}$ in the reciprocal lattice: apart from that, the phases of the Bloch functions at different $\mathbf{k}$ points are unrelated and completely arbitrary. Our phase choice implies for the u's:

$$u_s^{(\lambda)}(\mathbf{r},\mathbf{k}+\mathbf{G})=e^{-i\mathbf{G}\cdot\mathbf{r}}u_s^{(\lambda)}(\mathbf{r},\mathbf{k}), \tag{3}$$

where $\mathbf{G}$ is a translational reciprocal lattice vector.

Atomic Hartree units are adopted throughout. The Fock operator is therefore

$$F^{(\lambda)}=-\frac{1}{2}\nabla^2+V^{(\lambda)}, \tag{4}$$

where the periodic potential is *nonlocal*, and depends on λ, both in its bare (electron-ion) and self-consistent (Coulomb and exchange) terms. Taking advantage of translational symmetry, this operator is usually diagonalized one $\mathbf{k}$ vector at a time. Supposing there are n electrons per cell, only the lowest $n/2$ HF orbitals are relevant for electronic ground-state properties of a closed shell insulator. In any practical implementation the Fock operator is diagonalized over a discrete $\mathbf{k}$-point set: in the framework of the HF method, this heuristic approach has some significance as a matter of principle. Suppose in fact we use a uniform mesh with $N=N_1N_2N_3$ points along the primitive $\mathbf{G}_i$ reciprocal lattice vectors:

$$\mathbf{k}_{j_1,j_2,j_3}=\frac{j_1}{N_1}\mathbf{G}_1+\frac{j_2}{N_2}\mathbf{G}_2+\frac{j_3}{N_3}\mathbf{G}_3, \tag{5}$$

where $j_i=0,\ldots,N_i-1$. A moment of reflection shows that the approach is completely equivalent to studying a *finite* system of N cells with periodic boundary conditions. At variance with DFT, the HF method provides the electronic ground state as an explicit many-body wave function—in the form of a single Slater determinant—for the large system of nN electrons. We may write this wave function Ψ in the form of an antisymmetrized product of N small determinants of size n, i.e.,

$$\Psi^{(\lambda)}\propto\mathsf{A}\prod_{j_1,j_2,j_3}|\psi_1^{(\lambda)}(\mathbf{k}_{j_1,j_2,j_3})\overline{\psi}_1^{(\lambda)}(\mathbf{k}_{j_1,j_2,j_3})\cdots \times\psi_{n/2}^{(\lambda)}(\mathbf{k}_{j_1,j_2,j_3})\overline{\psi}_{n/2}^{(\lambda)}(\mathbf{k}_{j_1,j_2,j_3})|, \tag{6}$$

where A is the antisymmetrizer, and the electron coordinates are omitted from now on to simplify notations. The determinants of the ψ functions are simply related—through the plane-wave factors of Eq. (2)—to determinants of the u's. These determinants are useful in order to arrive at a very compact expression for $\Delta\mathbf{P}_{\rm el}$. We introduce a special notation for them:

$$|\Phi^{(\lambda)}(\mathbf{k})\rangle=\frac{1}{\sqrt{n!}}|u_1^{(\lambda)}(\mathbf{k})\,\overline{u_1^{(\lambda)}}(\mathbf{k})\ldots u_{n/2}^{(\lambda)}(\mathbf{k})\,\overline{u_{n/2}^{(\lambda)}}(\mathbf{k})|, \tag{7}$$

where the u's are the periodic factors of the $n/2$ lowest crystalline orbitals, Eq. (2). The main formula of the Berry phase theory, due to King-Smith and Vanderbilt,[1] can then be cast as

$$\Delta\mathbf{P}_{\rm el}=-\frac{i}{(2\pi)^3}\int d\mathbf{k}[\langle\Phi^{(1)}(\mathbf{k})|\nabla_{\mathbf{k}}\Phi^{(1)}(\mathbf{k})\rangle -\langle\Phi^{(0)}(\mathbf{k})|\nabla_{\mathbf{k}}\Phi^{(0)}(\mathbf{k})\rangle], \tag{8}$$

where the integral is taken over the unit reciprocal cell.

Most of the expressions reported so far for $\Delta\mathbf{P}_{\rm el}$ were given in terms of the individual u orbitals.[1,2] Within the HF scheme, they are all equivalent to Eq. (8), first proposed in Ref. 5. The equivalence proof is rather simple, upon expansion of $\Phi^{(\lambda)}(\mathbf{k})$ back in terms of the orbitals. This will also be clear from the discretized version of Eq. (8), discussed in the next section. Among other merits, the expression of Eq. (8) provides the link between the HF theory of polarization presented here, and the one for correlated wave functions, due to Ortíz and Martin.[21]

III. NUMERICAL IMPLEMENTATION

A. Discretization

In the present implementation we discretize the reciprocal-cell integral of Eq. (8) with a finite sum over a three-dimensional mesh similar to that used in the self-consistent electronic structure calculation, Eq. (5). We start performing a linear change of variables:

$$\mathbf{k}=\zeta_1\mathbf{G}_1+\zeta_2\mathbf{G}_2+\zeta_3\mathbf{G}_3. \tag{9}$$

The component of $\Delta\mathbf{P}_{\rm el}$ along say $\mathbf{G}_3$ is then, from Eq. (8),

$$\mathbf{G}_3\cdot\Delta\mathbf{P}_{\rm el}=-\frac{i}{\Omega}\int d\zeta_1 d\zeta_2 d\zeta_3\left[\left\langle\Phi^{(1)}(\boldsymbol{\zeta})\middle|\frac{\partial}{\partial\zeta_3}\Phi^{(1)}(\boldsymbol{\zeta})\right\rangle -\left\langle\Phi^{(0)}(\boldsymbol{\zeta})\middle|\frac{\partial}{\partial\zeta_3}\Phi^{(0)}(\boldsymbol{\zeta})\right\rangle\right], \tag{10}$$

and the integral is performed over the unit cube in the $\boldsymbol{\zeta}$ variable, whose N mesh points are $\boldsymbol{\zeta}_{j_1,j_2,j_3}$. A straightforward discretization would provide each of the two integrals in Eq. (10) in the form:

$$\int d\zeta_1 d\zeta_2 d\zeta_3 \left\langle \Phi^{(\lambda)}(\boldsymbol{\zeta}) \left| \frac{\partial}{\partial \zeta_3} \Phi^{(\lambda)}(\boldsymbol{\zeta}) \right\rangle \right.$$
$$\simeq \frac{1}{N_{j_1,j_2,j_3}} \sum \left\langle \Phi^{(\lambda)}(\boldsymbol{\zeta}_{j_1,j_2,j_3}) \left| \frac{\partial}{\partial \zeta_3} \Phi^{(\lambda)}(\boldsymbol{\zeta}_{j_1,j_2,j_3}) \right\rangle \right.$$
$$\simeq \frac{1}{N_1 N_2} \sum_{j_1,j_2,j_3} \times [\langle \Phi^{(\lambda)}(\boldsymbol{\zeta}_{j_1,j_2,j_3}) | \Phi^{(\lambda)}(\boldsymbol{\zeta}_{j_1,j_2,j_3+1}) \rangle - 1]. \quad (11)$$

This naive expression cannot be used as such, since the eigenfunctions are obtained by numerical diagonalization, and their phase at different $\mathbf{k}$ points is chosen essentially at random by the diagonalization routine. A different discretization algorithm must be used, in order to make such phase arbitrariness harmless: the solution, explained, e.g., in Ref. 2, is to replace

$$-i[\langle \Phi^{(\lambda)}(\boldsymbol{\zeta}_{j_1,j_2,j_3}) | \Phi^{(\lambda)}(\boldsymbol{\zeta}_{j_1,j_2,j_3+1}) \rangle - 1]$$
$$\rightarrow \mathrm{Im} \ln \langle \Phi^{(\lambda)}(\boldsymbol{\zeta}_{j_1,j_2,j_3}) | \Phi^{(\lambda)}(\boldsymbol{\zeta}_{j_1,j_2,j_3+1}) \rangle, \quad (12)$$

where Eq. (3) must be enforced in expressing $\Phi^{(\lambda)}(\boldsymbol{\zeta}_{j_1,j_2,N_3})$ through $\Phi^{(\lambda)}(\boldsymbol{\zeta}_{j_1,j_2,0})$. In other words, only N_3 independent diagonalization must be performed over a given line, *not* N_3+1. The discretized integral then reads

$$-i \int d\zeta_1 d\zeta_2 d\zeta_3 \left\langle \Phi^{(\lambda)}(\boldsymbol{\zeta}) \left| \frac{\partial}{\partial \zeta_3} \Phi^{(\lambda)}(\boldsymbol{\zeta}) \right\rangle \right.$$
$$\simeq \frac{1}{N_1 N_2} \mathrm{Im} \ln \prod_{j_1,j_2,j_3} \langle \Phi^{(\lambda)}(\boldsymbol{\zeta}_{j_1,j_2,j_3}) | \Phi^{(\lambda)}(\boldsymbol{\zeta}_{j_1,j_2,j_3+1}) \rangle. \quad (13)$$

We are left with the problem of evaluating the overlap between two Slater determinants, each built of an orthonormal set of periodic spin orbitals, but where the two sets overlap. According to a well known theorem, the overlap between the two determinants equals the determinant of the overlap matrix between the two sets of spin orbitals. The latter is the square of the determinant of the overlap matrix S between the doubly occupied space orbitals:

$$\langle \Phi^{(\lambda)}(\boldsymbol{\zeta}) | \Phi^{(\lambda)}(\boldsymbol{\zeta}') \rangle = \det^2 S^{(\lambda)}(\boldsymbol{\zeta}, \boldsymbol{\zeta}'),$$
$$S^{(\lambda)}_{s,s'}(\boldsymbol{\zeta}, \boldsymbol{\zeta}') = \langle u^{(\lambda)}_s(\boldsymbol{\zeta}) | u^{(\lambda)}_{s'}(\boldsymbol{\zeta}') \rangle. \quad (14)$$

B. Expansion over a localized basis

The HF crystalline orbitals used in the previous expressions have been obtained from the CRYSTAL95 code,[19] in linear combination of atomic orbitals (LCAO) form: more precisely they are expanded over a set of contracted Gaussian functions $\varphi_\mu(\mathbf{r})$, centered at sites $\mathbf{s}_\mu$, where $\mu = 1, \ldots, M$ is a basis label in the primitive cell. If $\mathbf{R}_l$ is a generic lattice translation, the occupied crystalline HF orbitals take the form

$$\psi^{(\lambda)}_s(\mathbf{r}, \mathbf{k}) = \frac{1}{\sqrt{L}} \sum_{\mu=1}^{M} \alpha^{(\lambda)}_{\mu,s}(\mathbf{k}) \sum_{l=1}^{L} e^{i\mathbf{k}\cdot\mathbf{R}_l} \varphi_\mu(\mathbf{r} - \mathbf{s}_\mu - \mathbf{R}_l), \quad (15)$$

where L is the infinite number of cells in the crystal and the α coefficients are provided by the diagonalization routine at a given $\mathbf{k}$, with an arbitrary phase choice. A typical overlap matrix element is therefore

$$\langle u^{(\lambda)}_s(\mathbf{k}) | u^{(\lambda)}_{s'}(\mathbf{k}') \rangle$$
$$= \sum_{\mu,\mu'=1}^{M} \alpha^{(\lambda)*}_{\mu,s}(\mathbf{k}) \alpha^{(\lambda)}_{\mu',s'}(\mathbf{k}') \times \sum_{l=1}^{L} e^{i\mathbf{k}'\cdot\mathbf{R}_l} \langle \varphi_\mu(\mathbf{r} - \mathbf{s}_\mu) | e^{-i\Delta\mathbf{k}\cdot\mathbf{r}} | \varphi_{\mu'}(\mathbf{r} - \mathbf{s}_{\mu'} - \mathbf{R}_l) \rangle, \quad (16)$$

where $\Delta\mathbf{k} = \mathbf{k}' - \mathbf{k}$. The integral on the right-hand side of Eq. (16) does not depend on $\mathbf{k}$ or $\mathbf{k}'$, but only on their difference $\Delta\mathbf{k}$. As the $\mathbf{k}$-point mesh is regular and $\mathbf{k}'$ is contiguous to $\mathbf{k}$, $\Delta\mathbf{k}$ can assume only the three values $\Delta\mathbf{k}_1$, $\Delta\mathbf{k}_2$, and $\Delta\mathbf{k}_3$, where

$$\Delta\mathbf{k}_1 = \mathbf{G}_1 / N_1,$$
$$\Delta\mathbf{k}_2 = \mathbf{G}_2 / N_2, \quad (17)$$
$$\Delta\mathbf{k}_3 = \mathbf{G}_3 / N_3.$$

Besides the α coefficients, the basic ingredients of Eq. (16) are therefore the matrix elements of suitable plane waves over the localized basis. The $\mathbf{R}_l$ summation is truncated when the overlap between the $\varphi_\mu(\mathbf{r} - \mathbf{s}_\mu)$ and the $\varphi_{\mu'}(\mathbf{r} - \mathbf{s}_{\mu'} - \mathbf{R}_l)$ functions is smaller than a given threshold T. When $T = 10^{-6}$ is used, the summation is fully converged. With this value of T, and with the basis set described in Table I [case (b) of Table II], about 4×10^5 integrals have to be calculated. The algorithm adopted for their evaluation is presented in the Appendix.

IV. ELECTRONIC STRUCTURE

The electronic properties of $KNbO_3$ have been thoroughly investigated in the literature within DFT,[11–15] but no previous analysis exists at the *ab initio* HF level. A detailed study of the calculated HF properties of this material is therefore in order as a preliminary work before dealing with macroscopic polarization. As a first step we have optimized an all-electron basis set. Then we have switched to a pseudopotential framework, using Hay-Wadt small core pseudopotentials[22] for K and Nb (and all electrons for oxygen[23]), optimizing the basis set again, and checking that all ground-state properties—polarization included, as discussed in Sec. VI—remain stable. All of the results reported in this section refer to the pseudopotential basis set described in Table I.

We have considered two structures, corresponding to $\lambda = 0$ and $\lambda = 1$, both illustrated in Fig. 1, and which share the same tetragonal unit cell. We have chosen the structural parameters measured[24] at 270 °C: $a = 3.997$ Å, and $c = 4.063$ Å. The $\lambda = 0$ structure is centrosymmetric, and is the same

TABLE I. Exponents and coefficients of the contracted Gaussian basis set adopted in the present study for Nb and K, in conjunction with small core pseudopotentials (Ref. 22). The coefficients multiply individually normalized Gaussian type orbitals (GTO's).

	Niobium			Potassium		
		Coeff.			Coeff.	
Shell	exp.	$s(d)$	p	exp.	$s(d)$	p
sp	3.5654	0.2637	-0.2001	7.5060	-0.0209	-0.0495
	2.7049	-0.7566	0.1230	2.3710	-0.4292	0.0266
	0.7705	1.1452	1.3226			
sp	0.2328	1	1	0.9130	1	1
sp				0.3092	1	1
d	21.3176	-0.0138		0.4340	1	
	1.2386	2.8724				
	0.4222	4.3807				
d	0.2060	1				

which was called ''ideal'' in Ref. 6. The $\lambda=1$ structure is the ferroelectric experimental one, where the atoms are displaced off center. We keep the origin fixed on Nb, and the remaining displacements are then,[24] in units of c: -0.023 (K), -0.040 (O_I), and -0.042 (O_{II}), where ''O_I'' refers to top and bottom oxygen ions and ''O_{II}'' refers to the four oxygen ions in the basal plane of the octahedron.

The electronic structure of this material has been somewhat discussed in the past; it is now well assessed that $KNbO_3$ is rather far from the extreme ionic limit, and is instead an intermediate ionic/covalent compound.[9,25] Further insight is provided—quite naturally within the present LCAO approach—by the Mulliken population analysis data: as usual, such analysis is not exempt from ambiguities, but it is very useful in order to investigate the overall bonding features. The net Mulliken charges for the $\lambda=0$ ($\lambda=1$) structure are $+0.99$ ($+0.99$), $+3.23$ ($+3.26$), -1.39 (-1.42), and -1.42 (-1.42) for K, Nb, O_I, and O_{II}, respectively. These data show first of all that the ferroelectric distortion has an irrelevant effect on the (static) ionic charges. Inspection of the figures show that the K atom is completely ionized, while the ionicity of both Nb and O is considerably weaker than the formal charge state of these ions ($+5$ and -2, respectively). The two Nb sp shells (see Table I) contain about eight electrons (7.97), i.e., those required to fill the 4s and 4p orbitals. The 5s orbital is then empty. The 1.77 electrons resulting from the difference between the formal charge ($+5$) and the Nb net charge ($+3.23$) are allocated in the 4d orbitals (1.04 and 0.73 $|e|$ in e_g and t_{2g} orbitals, respectively). By considering the ideal ionic state as a reference, the most important modification is a back donation from oxygen p to Nb d levels. As Nb d orbitals are quite diffuse (the exponent of the most diffuse function is 0.206 bohr^{-2}), an important overlap takes place between O 2p and Nb 4d (e_g) orbitals, which favors back donation. The Nb-O population is large and positive (0.14 $|e|$ for each Nb-O couple), indicating that this bond has large covalent components. The Nb-K, K-O, and O-O bond population, on the contrary, are negligibly small (we recall that covalent and ionic bonds are characterized by large and very small or null bond populations, respectively; short range repulsions give rise to small negative terms). The population of the d polarization functions on oxygen in $KNbO_3$ is extremely small (0.02 $|e|$); these functions, however, play a fundamental role in the ferroelectric instability (see next section).

For comparison purposes, we quote the Mulliken population data of another perovskite compound, $KNiF_3$.[26] The net charges are $+1.00$ (K), $+1.97$ (Ni), -0.96 (F); the Ni-F bond population (the equivalent of Nb-O in the present study), as well as the K-F and F-F ones, are smaller, in absolute value, than 0.01 $|e|$. These figures characterize $KNiF_3$ as much closer to the ideal ionic situation than $KNbO_3$: it is worth noting that $KNiF_3$ is *not* ferroelectric.

TABLE II. Basis set effect on the ferroelectric instability and on the calculated value of the spontaneous polarization ΔP. ΔE is the energy difference between the $\lambda=1$ and the $\lambda=0$ structures. ΔE is calculated with the shrinking factors $N_1=N_2=N_3=8$, and ΔP with $N_1=N_2=2$, $N_3=4$.

Case	Basis set	ΔE (mHa/cell)	ΔP (Cm^{-2})
(a)	all electrons	-3.138	0.3418
(b)	pseudo	-3.504	0.3419
(c)	as (b) but no d on K	-3.357	0.3376
(d)	as (b) but 1d shell on Nb	-1.602	0.3416
(e)	as (b) but no d on O	$+2.037$	0.3376
(f)	as (b) plus (c), (d), (e) modif.	$+2.116$	0.3340

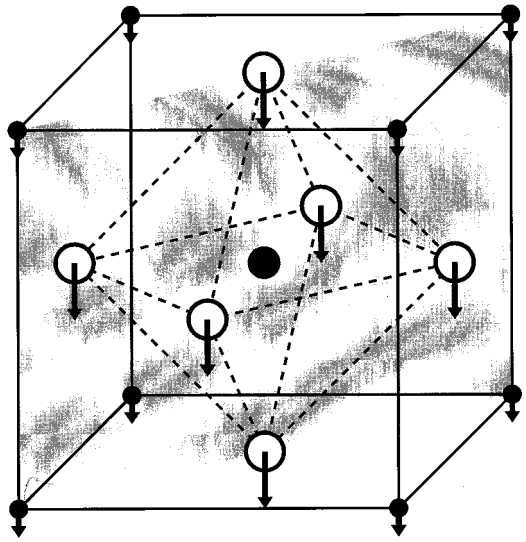

FIG. 1. Tetragonal structure of $KNbO_3$. The large black circle in the cube center represents Nb, the small black ones in the corners represent K, and white circles represent O. Internal displacements (indicated by arrows, and magnified by a factor 4) transform the ideal structure into the experimental one at 270 °C. Top and bottom O ions will be called O_I, while the four O ions in the basal plane of the octahedron will be called O_{II}. The shaded plane is the one chosen below for displaying the electronic density.

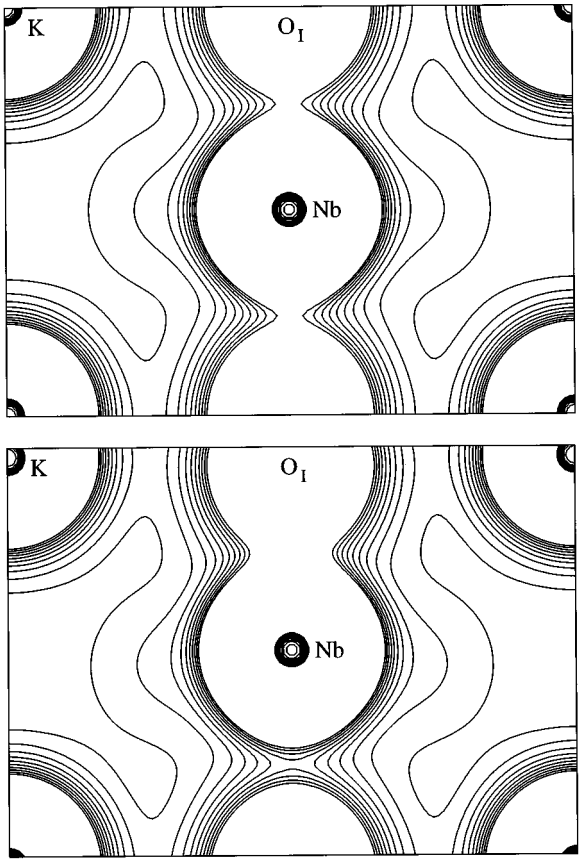

FIG. 2. Contour plot of the crystalline (pseudo) charge density in the (110) plane, which passes through K, Nb, and O_I atoms (see Fig. 1). Top panel: tetragonal centrosymmetric $\lambda=0$ structure; bottom panel: ferroelectric $\lambda=1$ structure. The separation between two contiguous isodensity curves is 0.01 e/bohr^3. The function is truncated in the core region at 0.1 e/bohr^3.

The features emerging from the Mulliken analysis are confirmed by the electronic total charge density maps, shown in Fig. 2 as contour plots in the (110) plane (this is the same plane which is shown as shaded in Fig. 1). Both densities, referring to the undistorted ($\lambda=0$) and distorted ($\lambda=1$) geometries, are quite different from a superposition of spherical densities; in order to enhance the deviation from the ionic model, the differences between the crystalline charge and the superposition of the spherical charges of free ions are plotted in Fig. 3. The figures confirm, first of all, that K atoms in the crystal are totally ionized, and virtually identical to free K^+ ions. Nb and O_I ions, as expected, are much different from their free shape, and display a conspicuous partly covalent bond, whose character is furthermore affected by the ferroelectric distortion; a build up of charge takes place in the Nb-O-Nb direction, whereas in the nonbonding directions a depletion of charge is observed (in the large area between vertical zero lines the difference function is negative).

The HF band structures for both $\lambda=0$ and $\lambda=1$ geometries are given in Fig. 4, and can be compared with the corresponding DFT ones available in the literature.[7,11] The Γ-X and Γ-Z dispersions would be identical in the cubic structure: the asymmetry in the left panel is therefore a fingerprint of the tetrahedral macroscopic strain. On top of this, the low symmetry ferroelectric distortion induces splittings and shifts in some of the highest valence bands (right panel), which indeed are important to the mechanism of ferroelectricity.[9] As expected the HF gap (about 8.4 eV) is much larger than experiment (3.3 eV), while the DFT one (1.3 eV) is much smaller. The analog holds for the overall bandwidth; the general appearance of the HF bands is however quite similar to the DFT ones, and the ferroelectric distortion induces band splittings of comparable magnitude [see, e.g., Fig. 1(a) in Ref. 9].

The total and projected density of states (DOS) provide additional information on the electronic structure. The highest occupied bands shown in Fig. 5 derive mostly from O 2p atomic orbitals and the lowest empty bands from Nb 4d orbitals. The highest valence DOS presents two main peaks, and Nb 4d AOs contribute mostly to the lowest shoulder; these qualitative features are very similar to those discussed in Refs. 6 and 11. We notice nonetheless that the previous investigations relied on a somewhat arbitrary partition of the crystal cell into atomic spheres plus a (large) interstitial region, whereas the present analysis naturally exploits the local-basis expansion. The overall valence DOS structure is also in qualitative agreement with the PES spectrum.[11] The e_g and t_{2g} contributions to the Nb d DOS is shown in Fig. 6. For simplicity reasons we have maintained the cubic symmetry symbols; in fact, although the degeneracies between d_{z^2} and $d_{x^2-y^2}$ in e_g, and between d_{xz} (or d_{yz}) and d_{xy} in t_{2g} are resolved in the tetragonal geometry, contributions to the DOS from functions belonging to the same group are extremely similar to each other. The usual bonding-antibonding splitting appears for both e_g and t_{2g} orbitals, which is sharper for the former as they are directed towards the oxygen atoms. The occupied e_g orbitals are much deeper in energy than the t_{2g} ones, because of the stabilizing interaction

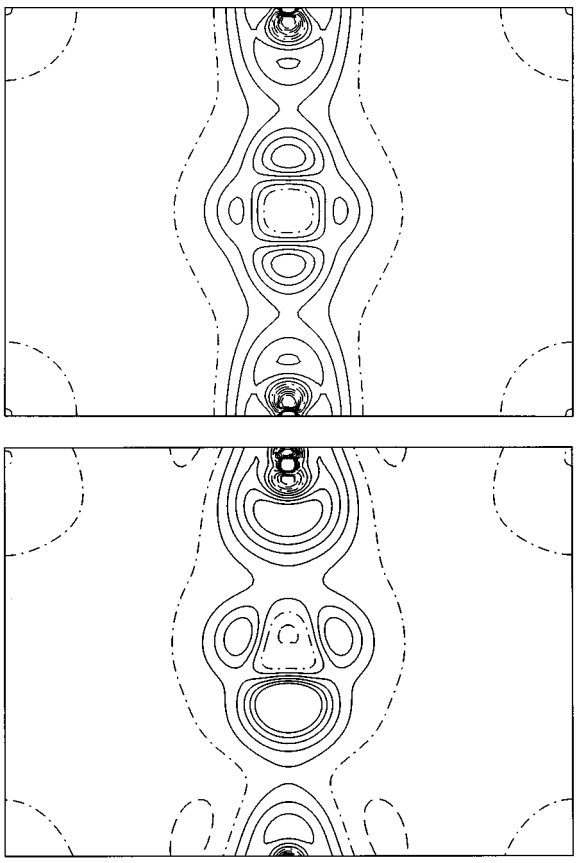

FIG. 3. Differences between the crystalline charge densities of Fig. 2, and the corresponding superpositions of spherical free-ion densities (K^+, Nb^{5+}, O^{2-}) obtained with the same basis set as used for the bulk. The separation between two contiguous isodensity curves is 0.008 e/bohr^3. The function is truncated in the core region at 0.04 e/bohr^3. Continuous, dashed, and dot-dashed lines indicate positive, negative, and zero values, respectively.

with oxygen orbitals. Finally, Fig. 7 shows the contribution of the two kinds of oxygen atoms to the undistorted and distorted structures; the most evident feature is the stabilization of O_I with respect to O_{II} in passing from the $\lambda=0$ to the $\lambda=1$ geometry, as a consequence of the reduced Nb-O_I distance and increased covalent interaction with Nb.

V. FERROELECTRIC INSTABILITY

In Table II the energy difference ΔE between the $\lambda=0$ and the $\lambda=1$ structures is reported, for several choices of the basis set. All results were generated using (i) a pseudopotential basis set for K and Nb (see Table I), and an all-electron basis set for oxygen;[23] (ii) computational condition defined as standard in the CRYSTAL95 manual;[19] (iii) shrinking factors $N_1=N_2=N_3=8$ in the SCF process. This choice provides well converged values of total energy and density matrix in all cases.

The most conspicuous message of Table II is that, in order for the ferroelectric instability to occur, *d* polarization functions have to be added to oxygen atoms. These basis functions allow the oxygen atom to develop a quadrupolar deformation, which is, in turn, the driving mechanism for the off center displacement of the Nb atom. As a matter of fact, early model approaches to the ferroelectric instability indeed emphasized—many years ago—the role of anisotropic oxygen polarizability.[27] The last column of Table II (better discussed in the forthcoming section) shows that, somewhat surprisingly, the same *d* polarization functions have little effect on the calculated value of the spontaneous polarization.

The role of oxygen *d* orbitals is also evident from Fig. 8, where the total energy versus Nb displacement (in units of *c*) is reported for basis sets (b) and (e) of Table II. The minimum at 0.05 is about 3.7 mhartree deep and disappears when *d* orbitals on oxygen are removed. A similar but less intense stabilization effect is due to the external diffuse *d* shell on Nb [case (b) and (d) in Table II].

The actual calculated depth of the broken-symmetry mini-

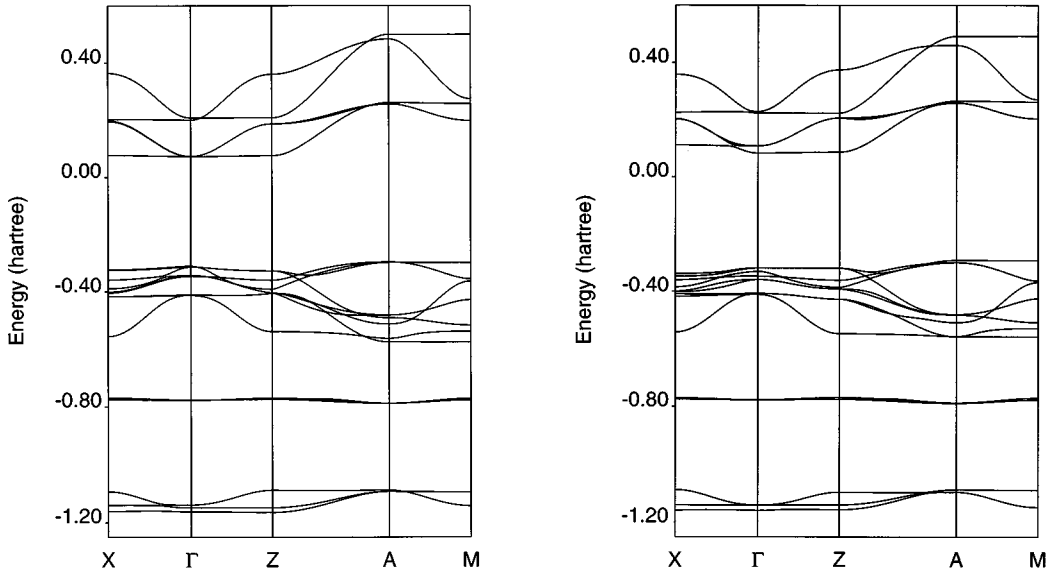

FIG. 4. Energy bands of $KNbO_3$ in the tetragonal centrosymmetric $\lambda=0$ structure (left panel), and in the corresponding ferroelectric $\lambda=1$ structure (right panel). The maximum of energy in the valence-band occurs at *A*; starting from the bottom, the three groups of valence bands derive mostly from O 2*s*, K 3*p*, and O 2*p* atomic states, respectively. The zero of energy is arbitrary.

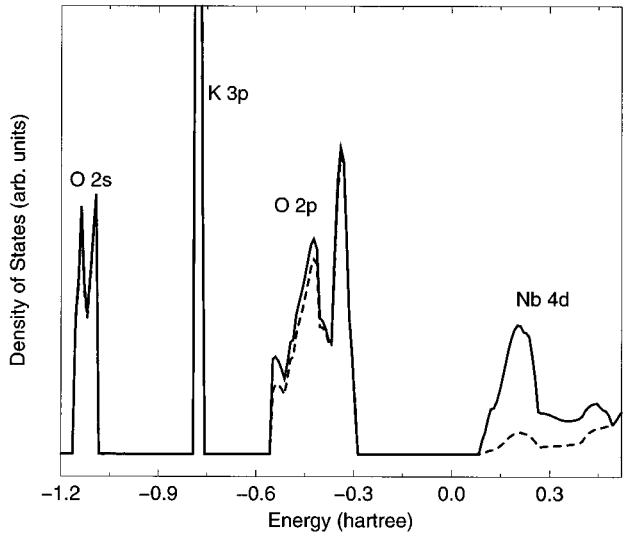

FIG. 5. Valence (negative energies) and conduction density of states (DOS) at the ($\lambda=1$) distorted experimental geometry, referred to as an arbitrary energy zero. We show the total DOS (solid line), and also a partial DOS, where the projection over the Nb 4*d* orbitals is subtracted from the total DOS (dashed line).

mum has been discussed by some authors within DFT. This depth is very sensitive to the volume at which the calculation is performed, and none of the existing calculations is precisely comparable to ours. However, the figures reported in Ref. 12 indicate a depth of a few mRy when the experimental cell volume is used (as it is done here): this compares quite well to our finding of 3.7 mhartree.

VI. MACROSCOPIC POLARIZATION

As emphasized in the modern theory of polarization[2] and throughout this work, $\Delta\mathbf{P}_{\mathrm{el}}$ is by definition the electronic current which flows through the crystal during the ferroelectric distortion. With reference to Fig. 2, we need to access the macroscopic current traversing the crystal cell while the ions

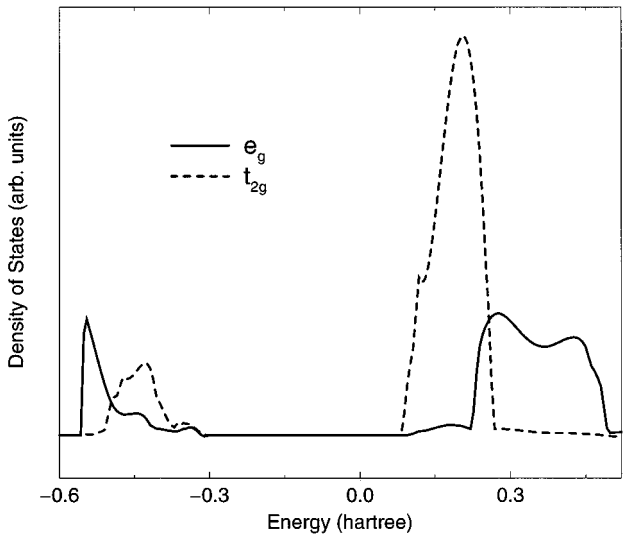

FIG. 6. Nb 4*d* contribution to the total DOS. The full line is the $d_{z^2}+d_{x^2-y^2}$ contribution; the dashed line refers to the other *d* orbitals.

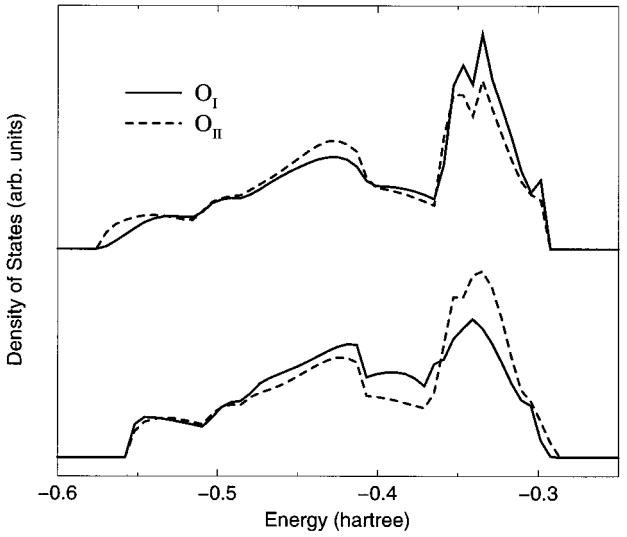

FIG. 7. Apical (O_I) and equatorial (O_{II}) oxygen contribution to the valence DOS. The upper and lower curves refer to the tetragonal undistorted ($\lambda=0$) and distorted ($\lambda=1$) geometries, respectively.

are continuously (and adiabatically) displaced from the top-panel geometry to the bottom one. Such integrated current is evaluated as a Berry phase of the Slater determinant. Contrary to a widespread belief—shared by many textbooks—there is no hope of recovering the value of $\Delta\mathbf{P}_{\mathrm{el}}$ from the electronic charge density itself. This latter quantity in fact only depends on the modulus of the wave function, where the relevant phase information is irretrievably deleted.

Spontaneous polarization $\Delta\mathbf{P}$ is a vector aligned to the internal atomic displacements; with reference to Fig. 1, it is vertical and directed from bottom to top. Since $\Delta\mathbf{P}$ horizontal components resulted to be numerically equal to zero in all of our calculations, from now on we indicate the spontane-

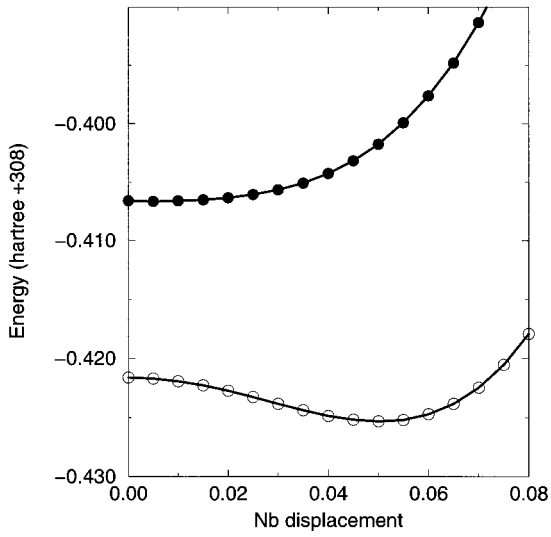

FIG. 8. Total energy versus [001] displacement of Nb (in units of the *c* lattice parameter), starting from the $\lambda=0$ tetragonal structure; K and O are kept fixed in their original $\lambda=0$ position. Open and full circles refer to basis sets with and without *d* orbitals on oxygen [cases (b) and (e) in Table II]. The energy difference at zero Nb displacement is 0.015 hartree, and is due to the additional variational freedom provided by *d* functions on oxygen.

TABLE III. Dependence of spontaneous polarization on N_1, N_2, and N_3, the shrinking factors for the reciprocal lattice vectors $\mathbf{G}_1$, $\mathbf{G}_2$, and $\mathbf{G}_3$, respectively. $\Delta P\%$ is the percentage difference in each set with respect to the most accurate result.

N_1	N_2	N_3	$N=N_1N_2N_3$	ΔP (Cm^{-2})	$\Delta P\%$
2	2	2	8	0.3248	+6.58
2	2	4	16	0.3419	+1.65
2	2	8	32	0.3463	+0.39
2	2	16	64	0.3474	+0.08
2	2	32	128	0.3476	
2	2	2	8	0.3248	−2.43
4	4	2	32	0.3172	−0.03
8	8	2	128	0.3171	
4	4	8	128	0.3385	

ous polarization value only through its modulus ΔP. The result obtained at the experimental distorted geometry is $\Delta P = 0.34\ \mathrm{Cm}^{-2}$ (see last entry in Table III), which is very close to the experimental value ($0.37\ \mathrm{Cm}^{-2}$, see Refs. 28, 29, and 10) and to previous theoretical results based on LDA methods (0.35, 0.33, and $0.40\ \mathrm{Cm}^{-2}$ as reported in Refs. 6, 10, and 8, respectively).

Our result was generated using the same computational conditions (i)–(iii) given in the previous section (more severe conditions do not alter the final result for ΔP), and a 128 **k**-point mesh ($N_1=N_2=4; N_3=8$) in the numerical evaluation of the integral in Eq. (8). The convergence of ΔP as a function of the number of **k** points used to evaluate such an integral is documented in Table III. In the plane orthogonal to the polarization direction, shrinking factors $N_1=N_2=4$ are sufficient to provide values very close to the converged one; in the polarization direction the convergence is slower, and at least $N_3=8$ is required in order to reduce the error to below 1%.

The effect of various variational basis sets on ΔP are summarized in Table II. In a preliminary calculation, an all-electron basis set was used, consisting of 22, 32, and 18 AO's for K, Nb, and O, respectively, grouped in 1 s, 4 sp, 1 d (K), 1 s, 4 sp, 3 d (Nb) and 1 s, 3 sp, 1 d (O) shells. The most diffuse sp functions were optimized individually in the bulk; this basis set is of very high quality, but also quite expensive; an equivalent pseudopotential basis set was then optimized for K and Nb, which is reported in Table I, whereas for oxygen the all-electron basis set was maintained. The comparison of first and second lines of Table II shows that the pseudopotential basis set reproduces quite accurately the all-electron data for ΔP; also ΔE is reproduced to within 10%. The other entries in the table show that ΔP is very stable with respect to simplifications of the basis set, such as the removal of d orbitals on K and O, or the reduction of the basis for the Nb 4d electrons from two d shells (3-1 G contraction) to a single d shell (3 G contraction).

As a final point, we investigated the linearity of spontaneous polarization as a function of the ferroelectric distortion; ΔP was evaluated in the interval $0 \leqslant \lambda \leqslant 2.5$ and the results are shown in Fig. 9. It turns out that ΔP remains approximately linear also for relatively high distortions; a second order correction becomes important only for the unphysical value $\lambda > 1.5$.

VII. DISCUSSION AND CONCLUSIONS

We have presented a thorough analysis of the electronic ground-state properties of $KNbO_3$ within the *ab initio* HF approach. The most important message emerging from the present study is that for this intermediate ionic-covalent compound the HF approach is very accurate, and basically enjoys the same predictive power as DFT. The latter approach, according to many published works, is well known to be extremely accurate in describing the electronic properties of this benchmark material.

As quoted in Sec. I, the HF approach was used so far only once in dealing with macroscopic polarization. The case study was ZnO, a simple (nonferroelectric) oxide.[5] Despite having a mixed ionic-covalent character, ZnO *apparently* behaves like a trivial ''rigid-ion'' material as far as polarization

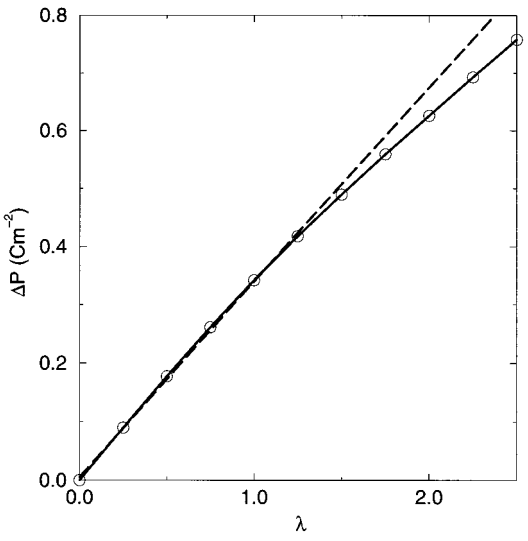

FIG. 9. Spontaneous polarization ΔP as a function of the magnitude λ of the ferroelectric distortion; $\lambda = 1$ corresponds to the experimental geometry of the ferroelectric structure at 270 °C. The dashed straight line was obtained interpolating the ΔP values in the interval $0 \leqslant \lambda \leqslant 1.25$.

is concerned. The subtle reasons for this are thoroughly discussed in Ref. 5, where it is also found that the DFT and HF approaches provide similar and accurate values when the polarization induced by sublattice displacements is addressed. However—as clearly stated in the conclusions of Ref. 5—such scheme independence was possibly *not* expected for other, more complex, materials.

In the present work we find that the calculated spontaneous polarization of $KNbO_3$ in its tetragonal ferroelectric phase is in very good agreement with the experiment, and with the existing DFT calculations as well.[7–10] This is not at all a trivial finding. In fact, we presently understand[9,25] the large value of the polarization in this material as due to a strong interaction of the highest occupied states (mostly oxygen $2p$) with the lowest unoccupied ones (mostly Nb $4d$). One would naively expect that such mixing effects are strongly affected by the energy position of the relevant bands. Given that the HF energy gap is very much larger than the DFT one, a very similar value of the calculated polarization could not be taken for granted beforehand. The reasons for the substantial equivalence of the two schemes are difficult to assess: this would require a thorough comparison of the wave functions (and notably of their *phase*) within an identical basis set. At present, we may only conjecture that the unscreened exchange might enhance the interaction between the occupied states with the lowest unoccupied ones, which are energetically distant within HF; conversely within DFT the gap is smaller but the exchange is effectively screened.

The overall equivalence of HF and DFT when dealing with the spontaneous polarization of $KNbO_3$ is therefore an important and gratifying find. This fact, in addition to the findings of Ref. 5, supports the idea that the two schemes provide a physical description of about the same quality for materials having a mixed ionic-covalent character.

Among several other properties investigated in the present work, a very important one is the ferroelectric instability, for which our results are once more in overall agreement with DFT ones. The energy gain of the broken-symmetry distortion is very tiny, and the mechanism can be easily disrupted by playing with the technical ingredients. In Ref. 9 a certain fake potential was added to the Hamiltonian: this modification suppresses at the same time the structural instability *and* the large value of the spontaneous polarization. Within the present localized-basis calculation, we are able to suppress the structural instability by simply removing from the basis set some important functions: namely, d orbitals centered on oxygen atoms. But, somewhat surprisingly, this same removal does not affect the calculated polarization at all.

Finally, we wish to discuss the issue of the linearity of the calculated polarization as a function of the magnitude of the ferroelectric distortion. In agreement with Ref. 6, we find an extremely good linearity: this is a nontrivial fact, given that ferroelectricity is essentially a nonlinear phenomenon. Very recently, Wang *et al.*[10] have investigated the linearity issue in much detail within DFT and have found rather important nonlinearities. They do not consider our case of a tetragonal ''collective'' displacement (where the whole ferroelectric distortion is scaled), while they address the polarization induced by *individual* sublattice displacements. The linearity/nonlinearity issue remains an interesting and intriguing one. The study of the polarization induced by individual sublattice displacements, and in particular its nonlinearity within HF, is cleary beyond the scope of the present paper and will be addressed in a subsequent study.

ACKNOWLEDGMENTS

R.D. acknowledges support by the Human Capital and Mobility Program of the European Union under Contract No. CHRX-CT93-0155, by the Italian MURST (40%) and Italian CNR. R.R. acknowledges support by ONR Grant No. N00014-96-1-0689.

APPENDIX

The atomic orbitals (AO's) $\varphi_\mu(\mathbf{r}) \equiv \varphi_l^m(\mathbf{r})$ are normalized to one and are linear combinations of Gaussian type orbitals (GTO's) $\gamma_{nlm}(\mathbf{r})$:

$$\varphi_l^m(\mathbf{r}) = \sum_n c_{nl}\gamma_{nlm}(\mathbf{r}). \tag{A1}$$

The GTO's are defined as

$$\gamma_{nlm}(\mathbf{r}) = N_l^m(\alpha_{nl}) X_l^m(\mathbf{r}) e^{-\alpha_{nl} r^2}, \tag{A2}$$

where

$$N_l^m(\alpha_{nl}) = \left(\frac{(2-\delta_{m0})(l-|m|)!}{(l+|m|)!}\right)^{1/2} \times \left(\frac{(\alpha_{nl})^l 2^{2l}(2l+1)}{(2l+1)!!}\right)^{1/2} \left(\frac{2\alpha_{nl}}{\pi}\right)^{3/4} \tag{A3}$$

is a normalization factor. $X_l^m(\mathbf{r})$ is a real solid spherical harmonic, which can be expressed as

$$X_l^m(\mathbf{r}) = \sum_{t,u,v}^{(t+u+v=l)} D_l^m(t,u,v) x^t y^u z^v, \tag{A4}$$

where the coefficients $D_l^m(t,u,v)$ are easily generated through recursion relations.[3,30]

By using Eq. (A1), (A2), and (A4), the integral which appears on the right-hand side of Eq. (16) can be written as

$$\begin{aligned}\langle \varphi_\mu(\mathbf{r}-\mathbf{s}_\mu) | e^{-i\Delta\mathbf{k}_i\cdot\mathbf{r}} | \varphi_{\mu'}(\mathbf{r}-\mathbf{s}_{\mu'}-\mathbf{R}_l)\rangle \\ = \sum_{n,n'} c_{nl}c_{n'l'} N_l^m(\alpha_{nl}) N_{l'}^{m'}(\alpha_{n'l'}) \\ \times \sum_{t,u,v}^{(t+u+v=l)} \sum_{t',u',v'}^{(t'+u'+v'=l')} D_l^m(t,u,v) D_{l'}^{m'}(t',u',v') \\ \times I_x I_y I_z,\end{aligned} \tag{A5}$$

where I_x can be cast as (the notation has been simplified as follows: $\mathbf{s}_1=\mathbf{s}_\mu$; $\mathbf{s}_2=\mathbf{s}_{\mu'}+\mathbf{R}_l$; $\alpha_i=\alpha_{nl}$; $\alpha_j=\alpha_{n'l'}$)

$$\begin{aligned}I_x = \int dx\ (x-s_{1x})^t (x-s_{2x})^{t'} \\ \times e^{-\alpha_i(x-s_{1x})^2} e^{-\alpha_j(x-s_{2x})^2} e^{-i\Delta k_{ix} x}.\end{aligned} \tag{A6}$$

By using the Gaussian product theorem,[31] and after some algebraic manipulations,[18] the integral I_x reduces to

$$I_x = e^{-\omega_{ij}(s_{1x}-s_{2x})^2} e^{-i\Delta k_{ix} h_x} \sum_{n=0}^{t} \sum_{l=0}^{t'} \binom{t}{n} \binom{t'}{l} \times (-1)^{t+t'-n-l} s_{1x}^{t-n} s_{2x}^{t'-l} \sum_{m=0}^{n+l} \binom{n+l}{m} h_x^{n+l-m} \times \int dx\, x^m e^{-\alpha_{ij} x^2} e^{-i\Delta k_{ix} x}, \tag{A7}$$

where

$$\alpha_{ij} = \alpha_i + \alpha_j; \quad \omega_{ij} = \frac{\alpha_i \alpha_j}{\alpha_i + \alpha_j}; \quad \mathbf{h} = \frac{\alpha_i \mathbf{s}_1 + \alpha_j \mathbf{s}_2}{\alpha_i + \alpha_j}. \tag{A8}$$

The integral in Eq. (A7) is related to the H_m Hermite polynomials,[31] so that finally one gets

$$I_x = \left(\frac{\pi}{\alpha_{ij}}\right)^{1/2} e^{-\omega_{ij}(s_{1x}-s_{2x})^2} e^{-\Delta k_{ix}^2/4\alpha_{ij}} e^{-i\Delta k_{ix} h_x} \times \sum_{n=0}^{t} \sum_{l=0}^{t'} \binom{t}{n} \binom{t'}{l} (-1)^{t+t'-n-l} s_{1x}^{t-n} s_{2x}^{t'-l} \times \sum_{m=0}^{n+l} i^m \binom{n+l}{m} h_x^{n+l-m} \left(\frac{1}{2\alpha_{ij}^{1/2}}\right)^m H_m\left(-\frac{\Delta k_{ix}}{2\alpha_{ij}^{1/2}}\right). \tag{A9}$$

Substitution of Eq. (A9), and similar expressions for I_y and I_z, into Eq. (A5) provides the expression adopted for the evaluation of the general integral.[18]

[1] R. Resta, Ferroelectrics **136**, 51 (1992): R.D. King-Smith and D. Vanderbilt, Phys. Rev. B **47**, 1651 (1993); R. Resta, Europhys. Lett. **22**, 133 (1993).

[2] R. Resta, Rev. Mod. Phys. **66**, 809 (1994).

[3] C. Pisani, R. Dovesi, and C. Roetti, *Hartree-Fock Ab Initio Treatment of Crystalline Systems*, Lecture Notes in Chemistry Vol. 48 (Springer, Berlin, 1988).

[4] *Theory of the Inhomogeneous Electron Gas*, edited by S. Lundqvist and N.H. March (Plenum, New York, 1983).

[5] S. Massidda, R. Resta, M. Posternak, and A. Baldereschi, Phys. Rev. B **52**, R16 977 (1995).

[6] R. Resta, M. Posternak, and A. Baldereschi, Phys. Rev. Lett. **70**, 1010 (1993).

[7] R. Resta, M. Posternak, and A. Baldereschi, in *Materials Theory and Modelling*, edited by J. Broughton, P.D. Bristowe, and J. M. Newsam, MRS Symposia Proceedings No. 291 (Materials Research Society, Pittsburgh, 1993), p. 647.

[8] W. Zhong, R.D. King-Smith, and D. Vanderbilt, Phys. Rev. Lett. **72**, 3618 (1994).

[9] M. Posternak, R. Resta, and A. Baldereschi, Phys. Rev. B **50**, 8911 (1994).

[10] C.Z. Wang, R. Yu, and H. Krakauer, Phys. Rev. B **54**, 11 161 (1996).

[11] T. Neumann, G. Borstel, C. Scharfschwerdt, and M. Neumann, Phys. Rev. B **46**, 10 623 (1992).

[12] A.V. Postnikov, T. Neumann, G. Borstel, and M. Methfessel, Phys. Rev. B **48**, 5910 (1993).

[13] R.D. King-Smith and D. Vanderbilt, Phys. Rev. B **49**, 5828 (1994).

[14] A.V. Postnikov, T. Neumann, and G. Borstel, Phys. Rev. B **50**, 758 (1994).

[15] R. Yu and H. Krakauer, Phys. Rev. Lett. **74**, 4067 (1995).

[16] R.I. Eglitis, A.V. Postnikov, and G. Borstel, Phys. Rev. B **54**, 2421 (1996).

[17] S.C. Abrahams and E.T. Keeve, Ferroelectrics **2**, 129 (1971).

[18] S. Dall'Olio, thesis, University of Torino, Torino, 1996.

[19] R. Dovesi, V.R. Saunders, C. Roetti, M. Causà, N.M. Harrison, R. Orlando, and E. Aprà, CRYSTAL95 *User's Manual* (University of Torino, Torino, 1996).

[20] M.E. Lines and A.M. Glass, *Principles and Applications of Ferroelectrics and Related Materials* (Clarendon Press, Oxford, 1977).

[21] G. Ortíz and R.M. Martin, Phys. Rev. B **49**, 14 202 (1994).

[22] P.J. Hay and W.R. Wadt, J. Chem. Phys. **82**, 270 (1985); **82**, 284 (1985); **82**, 299 (1985).

[23] Ph. D'Arco, F. Freyria Fava, R. Dovesi, and V.R. Saunders, J. Phys.: Condens. Matter **8**, 8815 (1996).

[24] A.W. Hewat, J. Phys. C **6**, 1074 (1973).

[25] *Materials Theory, Simulations, and Parallel Algorithms*, edited by E. Kaxiras, J. Joannopolos, P. Vashista, and R. K. Kalia, MRS Symposia Proceedings No. 408 (Materials Research Society, Pittsburgh, 1996), p. 9.

[26] J.M. Ricart, R. Dovesi, C. Roetti, and V.R. Saunders, Phys. Rev. B **52**, 2381 (1995).

[27] R. Migoni, H. Bilz, and D. Baüerle, Phys. Rev. Lett. **37**, 1155 (1976).

[28] W. Kleemann, F.J. Schäfer, and M.D. Fontana, Phys. Rev. B **30**, 1148 (1984).

[29] M.D. Fontana, G. Métrat, J.L. Servoin, and F. Gervais, J. Phys. C **6**, 1074 (1973).

[30] V.R. Saunders, C. Freyria Fava, R. Dovesi, L. Salasco, and C. Roetti, Mol. Phys. **77**, 629 (1992).

[31] V.R. Saunders, in *Computational Techniques in Quantum Chemistry and Molecular Physics*, edited by G.H.F.D. Diercksen *et al.* (Reidel, Dordrecht, 1975), p. 347.